Phys Chem Minerals (2006) 33:723–731
DOI 10.1007/s00269-006-0124-8

ORIGINAL PAPER

In situ time resolved synchrotron powder diffraction study of thaumasite

Annalisa Martucci · Giuseppe Cruciani

Received: 30 May 2006 / Accepted: 9 October 2006 / Published online: 8 November 2006

Abstract Structural changes during dehydration and subsequent decomposition in thaumasite $Ca_3Si(SO_4)(CO_3)(OH)_6{\cdot}12\ H_2O$ were studied by *in situ* synchrotron powder diffraction between 303 and 1,098 K. Evolution of the crystal structure was observed through 28 structure refinements, by full profile Rietveld analysis performed in the $P6_3$ space group, between 300 and 417 K, whereupon the thaumasite structure was observed to breakdown. Within this temperature range, the cell parameters of thaumasite increased as a function of temperature in a nearly linear fashion up to about 393 K, at which temperature, a slight slope change was observed. Above 400 K, the thermogravimetric analysis revealed that the dehydration process proceeded very rapidly while the refined occupancy of water molecules dropped below a critical level, leading to instability in the thaumasite structure. At a same time, a remarkable change in the unit cell parameters occurring at about 417 K indicated that the crystal structure of thaumasite collapsed on losing the crystallization water and it turned amorphous. This result indicated that the dehydration/decomposition of thaumasite was induced by the departure of the crystallization water. At about 950 K, anhydrite and cristobalite crystallized from the thaumasite glass.

Keywords Thaumasite · Heating process · *In situ* powder diffraction · X-ray synchrotron radiation · Rietveld analysis

A. Martucci (✉) · G. Cruciani
Dipartimento di Scienze della Terra,
Sezione di Mineralogia, Petrografia e Geofisica,
Via Saragat 1, Ferrara 44100, Italy
e-mail: mrs@dns.unife.it

Introduction

Thaumasite is a naturally occurring mineral with a hexagonal structure (space group $P6_3$) and an ideal composition of $[Ca_3Si(OH)_6{\cdot}12\ H_2O]\ [(SO_4)(CO_3)]$, widely found as a secondary phase in mafic igneous and metamorphic rocks (Knill 1960; Hurlbut and Baum 1960). It often arises as fissure or vug-filler in basaltic rocks, where it appears to be deposited by circulating fluids and appears to be metasomatic. For example, thaumasite from Prata Porci in the Latian volcano (Federico 1970) and Mururoa in French Polynesia (Noack 1983), formed by reaction between basaltic rocks and seawater. Both occurrences are related to low-enthalpy geothermics, so that thaumasite acquires the status of a potentially significant geothermal index mineral.

Thaumasite is also reported to form at low temperatures (below 288 K) as a product and indicator of sulphate attack (TSA) of Portland cement, when there is an available source of CO_3^{2-} (Crammond 1985; Bensted 1999; Lachaud 1979).

The structure is based on columns of an ideal composition of $[Ca_3Si(OH)_6{\cdot}12\ H_2O]^{4+}$ running parallel to ***c***, between which, occur the sulphate SO_4^{2-} and carbonate CO_3^{2-} groups (Edge and Taylor 1971; Zemann and Zobetz 1981; Effenberger et al. 1983).

Thaumasite is a member of the ettringite group of hydrated calcium sulfates that also include ettringite, $[Ca_6Al_2(OH)_{12}{\cdot}24\ H_2O][(SO_4)_3{\cdot}2\ H_2O]$, bentorite, $[Ca_6[(Cr,Al)_2(OH)_{12}{\cdot}24\ H_2O][(SO_4)_3 2\ H_2O]$; charlesite, $[Ca_6(Al,\ Si)_2(OH)_{12}{\cdot}24\ H_2O]\{(SO_4)_2[B(OH)_4]{\cdot}2\ H_2O\}$; sturmanite, $[Ca_6[(Fe^{3+},Al)_2\ (OH)_{12}]\ 24\ H_2O]\{(SO_4)_2[B(OH)_4]{\cdot}2\ H_2O\}$; jouravskite, $[Ca_6\ [(Mn^{4+})_2\ (OH)_{12}{\cdot}24\ H_2O]\ [(SO_4)_2(CO_3)_2]$; and also the most recently

described, micheelsenite, $[(Ca,Y)_6Al(PO_3OH,CO_3)_2(OH)_{12}{\cdot}24\ H_2O)](CO_3)_2$ (McDonald et al. 2001) and carraraite $[Ca_6Ge_2(OH)_{12}\ 24\ H_2O]\ [(SO_4)_{2.16}(CO_3)_{1.84}]$ (Merlino and Orlandi 2001).

The similarity of its crystal structure to that of ettringite (space group P31c), despite their different space groups, has led to confusion in the past. Hence, their unit cells and diffraction patterns are also similar, particularly for the readily observed {100} and {110} reflections. Carpenter (1963) reported thaumasite as oriented overgrowths on ettringite and suggested a limited solid solution series between these phases on the basis of anomalies in the refractive index of the two minerals. Recently, Barnett et al. (2000) provided clear evidence for the existence of a solid solution between ettringite and thaumasite, and explained a possible discontinuity in terms of the differing crystallography of the two structures.

The peculiarity of thaumasite is that it is the only mineral known to contain silicon in sixfold coordination with hydroxyl $(OH)^-$ that is stable at ambient *P–T* conditions. The only other fully hydrated silica octahedron is found in the synthetic high-pressure dense magnesium silicate, phase D, $MgSi_2H_2O_6$ (Yang et al. 1997; Frost and Fei 1998). The octahedral coordination of Si by oxygen at ambient pressure conditions is known in many inorganic compounds, and can be explained by the presence of atoms with relatively high electronegativity, such as C, H or P (Edge and Taylor 1971) coordinated to the O atoms. These atoms draw electrons out of the Si–O bonds, thus lengthening them, decreasing their mutual repulsion, and allowing the increase in Si coordination number. A similar circumstance also occurs for F atoms, and the $Si(OH)_6^{2-}$ group can be linked to the SiF_6^{2-} group, which is readily formed at ordinary pressures.

Thermal decomposition of thaumasite was determined by static methods (step-wise heating and weight determination; Vogt 1938; Kirov and Poulieff 1968), by dynamic methods (TG /DTA analyses; Font-Altaba 1960; Federico 1970; Grubessi et al. 1986) and kinetic methods (Giampaolo 1986). Thaumasite is stable up to approximately 383 K, when it decomposes to form the disordered structure known as 'thaumasite glass'. This stability is greater than that of ettringite, in which the crystal lattice collapse is commonly encountered above 323–333 K, often depending upon the length of time the ettringite is maintained at these temperatures. Brough and Atkinson (2001), using micro-Raman spectroscopy, showed that no water loss was found for thaumasite at 373 K, even after prolonged heating. The authors explained the lack of any lattice collapse in thaumasite prior to decomposition as an indication that the water content is more strongly bound than in ettringite, even though both structures exhibit a hexagonal-type prism morphology.

Recently, thermal decomposition of thaumasite was studied by Drábik and Gáliková (2003), using multistep thermal analysis (TG/DTA) combining dynamic and isothermal heating from room temperature to 1,273 K. TG/DTA effects showed that the dehydration process occurred in the temperature range 373–403 K, whereas dehydroxylation and decalcination reactions were observed in the temperature regions 473–573 and 853–953 K, respectively.

Jacobsen et al. (2003) investigated the thermal expansion of thaumasite by single crystal X-ray diffraction (XRD), with structure refinements at 130 and 298 K and measurement of the unit-cell parameters at intervals of about 50 K in this temperature range. These authors found that most of the thermal expansion in the structure is accommodated by the lengthening of all (Ca–O) bonds and the R(O···O) hydrogen bond distances, causing the $[Ca_3Si(OH)_6(H_2O)_{12}]^{4+}$ columns to both expand and move apart.

The continuous structural behaviour of thaumasite upon heating above room temperature, has not been reported so far, presumably due to the low temperature at which thaumasite starts to dehydrate (about 383 K, according to Brough and Atkinson 2001) and the fast kinetics of structural breakdown which occurs almost in parallel with dehydration. These features make single crystal XRD non-applicable due to the difficulty of maintaining equilibrium conditions during a complete data collection. The above limitations can be easily overcome by using Rietveld structure analysis of temperature-resolved powder diffraction data collected with synchrotron radiation. A further advantage when using time resolved experiments, instead of dealing with a limited number of snapshots, is the possibility of gaining insights into the dynamics of the process and to record non-quenchable structural modifications.

The present investigation strives to give a more exhaustive picture of the thermal expansion and dehydration processes in thaumasite within the temperature range 303–417 K, extending the temperature range previously studied by Jacobsen et al. (2003). Full-profile Rietveld structure refinements at several temperatures in this range are reported to provide complete information on the structural and volume modifications, and the thermal expansion of thauma-

site undergoing thermal dehydration, with particular attention to dynamic and transient effects.

Experimental

All the experiments in the present study were performed on a thaumasite sample from the Upper New Street Quarry (West Paterson, NJ, USA). Thaumasite from this locality has been reported as occurring within interstitial spaces between the pillows of basaltic lavas that were extruded over a probable shallow wetland or lake (Peters 1984). A specimen from Paterson, NJ, was also used by Edge and Taylor (1971) for the single crystal structure determination of thaumasite.

Time resolved diffraction data were collected at the GILDA operating beamline at ESRF (Grenoble) in parallel Debye-Scherrer geometry, using a fixed wavelength of 0.68765 Å. The powder sample was packed into a 0.3 mm diameter Lindemann capillary, open at both ends, and heated *in situ,* using a hot air stream; a constant heating rate of 5 K/min was applied, and the sample was heated from 303 to 1,098 K. During the heating process, powder diffraction patterns were recorded on the 4 mm slit-delimited portion of a translating flat image plate (Norby 1997), which had a translation rate of 2.5 pixel/K with respect to the temperature increase. External standard LaB_6 was used to calibrate the wavelength, as well as to determine the zero-shift position, sample to detector distance, and tilting angle of the image plate detector. A three-dimensional plot of powder patterns (2θ–intensity–temperature) is shown in Fig. 1.

The TGA analyses were carried out on a TG Netzsch instrument (STA 409 PC model) by keeping 60.6 mg of sample under a constant flux of air, and using a heating rate of 5 K/min. The weight loss from 303 to 1,098 K was about 50%. Chemical analysis was performed by X-ray fluorescence spectroscopy (XRF) on a ThermoARL Advant'XP spectrometer by adopting a normalization procedure based on empirical curves calibrated against international standards (Traill–Lachance method). The results of the chemical analysis indicated that the sample composition was similar within the experimental error range, to that reported by Edge and Taylor (1971), which is in turn very close to the ideal one.

The structure refinements (by full profile Rietveld analysis) were performed in the $P6_3$ space group using the GSAS package (Larson and Von Dreele 2000), starting from the atomic positions found by Jacobsen et al. (2003). Since no evidence was found to support a change in symmetry on the powder pattern until decomposition at ~417 K, the same $P6_3$ space group as at room temperature was adopted in all the crystal structure refinements. In all refinements, the Bragg peak profile was modelled using a pseudo-Voigt function with a 0.01% cut-off of the peak intensity. The background curve was fitted using a Chebyschev polynomial with 24 variable coefficients. The 2θ-zero shift was accurately refined in all the patterns of the data set. One scale factor and the unit-cell parameters were allowed to vary for all histograms. In the final cycles, the refined structural parameters for each data histogram were the following: fractional coordinates for all atoms, occupancy factors for water molecules, and isotropic displacement factors. Occupancy factors and isotropic displacement factor coefficients were varied in alternate cycles. Reasonable values were obtained for C–O and S–O bond distances, left free in all the stages of refinement.

Final observed and calculated powder patterns for thaumasite at 303 K and 413 K are shown in Fig. 2. Lattice parameters and refinement details are reported

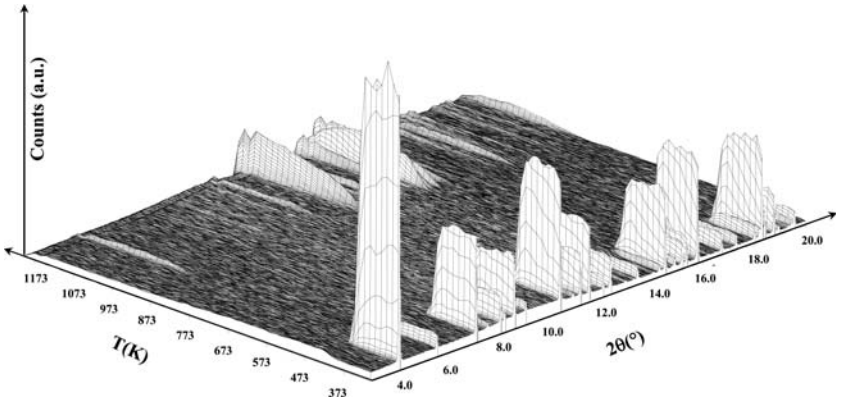

Fig. 1 Evolution of the XRPD patterns in the 4–20° 2θ interval as a function of the temperature (373–1173 K) during the *in situ* experiment

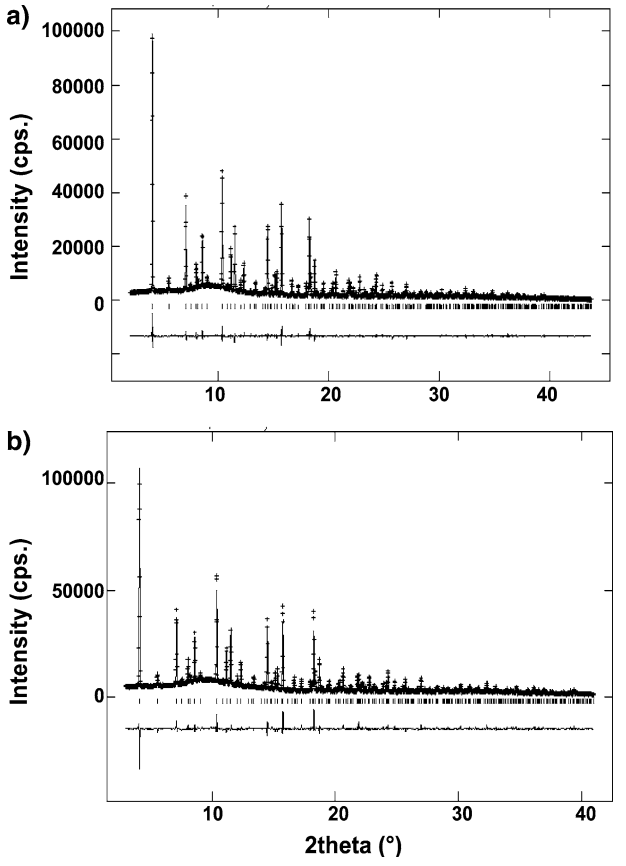

Fig. 2 Observed (*dotted upper line*), calculated (*solid upper line*), and difference (*solid lower line*) powder diffraction patterns of thaumasite at 303 K (**a**) and 413 K (**b**) from *in situ* data, respectively

in Table 1, atomic coordinates, occupancy and temperature factors are reported in Table 2; bond distances are in Table 3.

Table 1 Lattice parameters and refinement details for thaumasite at 303 K and 413 K from *in situ* data, respectively

Temperature (K)	303	413
Space group	$P6_3$	$P6_3$
a (Å)	11.0575(1)	11.0825(2)
C (Å)	10.4163(1)	10.4447(3)
V (Å)^3	1102.96(2)	1110.99(4)
α (deg)	90	90
β (deg)	90	90
γ (deg)	120	120
Refined pattern 2θ range (deg)	2.08–43.7	2.98–40.9
R_{wp} (%)	7.01	5.81
R_p (%)	5.15	4.26
R_F^2 (%)	10.6	13.5
N_o.of contributing reflections	528	444
N_{obs}	4,168	4,032
N_{var}	84	84

Table 2 Atomic coordinates and thermal parameters for thaumasite at 303 K and 413 K from *in situ* data, respectively

		303	413
Ca	*x/a*	0.1962(3)	0.1975(4)
	y/b	0.9895(4)	0.9909(7)
	z/c	0.2463(8)	0.231(5)
	Uiso	0.031(1)	0.019(1)
	Frac.	1.0	1.0
Si	*x/a*	0	0
	y/b	0	0
	z/c	–0.0039(16)	–0.025(6)
	Uiso	0.032(2)	0.023(3)
	Frac.	1.0	1.0
C	*x/a*	1/3	1/3
	y/b	2/3	2/3
	z/c	0.4674(23)	0.449(7)
	Uiso	0.007(6)	0.003(13)
	Frac.	1.0	1.0
S	*x/a*	1/3	1/3
	y/b	2/3	2/3
	z/c	0.9836(10)	0.977(6)
	Uiso	0.039(2)	0.042(4)
	Frac.	1.0	1.0
O1	*x/a*	0.3916(10)	0.3927(16)
	y/b	0.2287(10)	0.2367(17)
	z/c	0.2397(20)	0.226(6)
	Uiso	0.058(3)	0.024(5)
	Frac.	1.0	0.98(1)
O2	*x/a*	0.2605(10)	0.2555(20)
	y/b	0.4008(9)	0.4080(19)
	z/c	0.2535(16)	0.242(6)
	Uiso	0.060(4)	0.076(7)
	Frac.	1.0	0.96(2)
O3	*x/a*	0.0034(15)	–0.0018(21)
	y/b	0.3330(13)	0.3297(16)
	z/c	0.0591(18)	0.044(6)
	Uiso	0.037(4)	0.002(4)
	Frac.	1.0	0.96(2)
O4	*x/a*	0.0226(11)	0.0208(16)
	y/b	0.3584(12)	0.3656(15)
	z/c	0.4118(19)	0.390(5)
	Uiso	0.038(5)	0.028(5)
	Frac.	1.0	0.99(2)
O5	*x/a*	0.2055(6)	0.2085(13)
	y/b	0.6287(9)	0.6272(24)
	z/c	0.4633(8)	0.456(6)
	Uiso	0.036(3)	0.042(5)
	Frac.	1.0	1.0
O6	*x/a*	0.1926(7)	0.1954(15)
	y/b	0.6244(8)	0.6296(19)
	z/c	0.0414(7)	0.031(6)
	Uiso	0.032(3)	0.024(6)
	Frac.	1.0	1.0
O7	*x/a*	0.1181(11)	0.1211(18)
	y/b	0.1219(12)	0.1232(22)
	z/c	0.0964(15)	0.080(6)
	Uiso	0.040(5)	0.033(6)
	Frac.	1.0	1.0
O8	*x/a*	0.1429(10)	0.1465(15)
	y/b	0.1288(11)	0.1340(18)
	z/c	0.3879(15)	0.372(5)
	Uiso	0.017(4)	0.003(9)
	Frac.	1.0	1.0

Table 2 continued

		303	413
O9	*x/a*	1/3	1/3
	y/b	2/3	2/3
	z/c	0.8392(15)	0.832(6)
	Uiso	0.067(7)	0.026(8)
	Frac.	1.0	1.0

Table 3 Variation of the coordination polyhedra in thaumasite at 303 K and 413 K from *in situ* data, respectively

Bond	303	413
$[Ca_6(H_2O)_4]\ (OH)_4]^{2-}$ polyhedron	Ca–O1 2.45(1)	Ca–O1 2.49(2)
	Ca–O2 2.52(1)	Ca–O2 2.52(2)
	Ca–O3 2.37(2)	Ca–O3 2.42(2)
	Ca–O4 2.40(2)	Ca–O4 2.37(2)
	CaO7a 2.55(1)	CaO7a 2.57(2)
	Ca–O7d 2.41(1)	Ca–O7d 2.46(2)
	Ca–O8b 2.41(1)	Ca–O8b 2.43(2)
	Ca–O8d 2.51(1)	Ca–O8d 2.52(2)
Average $<^{VIII}$Ca-O>	2.455	2.471
$[Si(OH)_6]^{2-}$ octahedron	Si–O7 1.76(1) (×3)	Si–O7 1.74(2)(×3)
	Si–O8 1.82(1) (×3)	Si–O8 1.89(2) (×3)
Average $<^{VI}$Si-O>	1.796	1.818
$(SO)_4^{2-}$ tetrahedron	S–O6 1.50(1) (×3)	S–O6 1.48(1) (×3)
	S–O9 1.48(1)	S–O9 1.51(2)
Average $<^{IV}$S-O>	1.493	1.499
$(CO_3)^{2-}$ group	C–O5 1.26(1) (×3)	C–O5 1.23(1) (×3)
elevation of C	0.025 Å	0.056Å

Results and discussion

Refinements by ''in situ'' X-ray data: temperature-dependent variation of the unit cell parameters and structural modifications

The structure refinement by full profile Rietveld at room temperature confirm that the structure is based on columns of empirical composition $[Ca_3Si(OH)_6 \cdot 12\ H_2O]^{4+}$ running parallel to ***c***, with the sulphate and carbonate groups distributed in an ordered arrangement along the channels between the columns (Fig. 3). In agreement with Edge and Taylor (1971), our results indicate a distortion of the $Si(OH)_6^{2-}$ octahedron, which gives rise to three relatively short Si–O bonds (1.76 Å) on one side of the Si atom, and three long ones (1.83 Å) on the other. The average value <Si–O> = 1.796 Å is slightly larger than the average anhydrous six-coordinate Si–O bond value (1.794 Å) commonly observed in various high-pressure silicates (Ross et al. 1990; Horiuchi et al. 1982; Angel et al. 1989; Horiuchi et al. 1987) and shorter than the one found in the synthetic phase D $MgSi_2H_2O_6$ (Yang et al. 1997; Frost and Fei 1998).

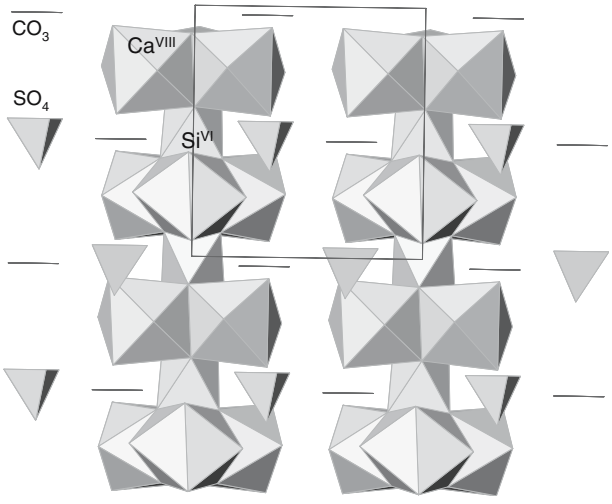

Fig. 3 Structure of thaumasite projected on (11–20)

The Ca–O bond distances in the square antiprism, which range from 2.37 to 2.55 Å, agree closely with those reported by Edge and Taylor (1971), as well as with the corresponding values in jouravskite (Granger and Protas 1969). The sulphate and carbonate groups give acceptable bond distances and temperature factors. The refinement indicates that the CO_3^{2-} groups show a slight deviation from planarity (0.02 Å) in the direction of the apical oxygen of sulphate. This value is usual for carbonate minerals, where C typically lies ~0.02 Å above the oxygen plane (Reeder 1983).

The stepwise dehydration process in thaumasite can be monitored by the variation of the lattice parameters *a*, *c* and cell volume (Table 4). Figure 4a–c reports the evolution of the cell volume and cell parameters during the *in situ* thermal burning of the thaumasite sample in the temperature range 303–417 K, at 5 K intervals. To allow a better comparison among the cell parameters adimensional values, have also been reported, defined as $V_{(T)}/V_{130}$, $a_{(T)}/a_{130}$ and $c_{(T)}/c_{130}$, these being the reference values obtained by Jacobsen et al. (2003) at 130 K (Fig. 4d). The thermal expansion along the *a*- and *c*-axis directions is very similar in the whole temperature range investigated. In particular, the cell parameters of thaumasite increase with increasing temperature in a nearly linear fashion up to about 393 K. As will be discussed later, this slope change is associated with the loss of water molecules, which occurs in this temperature range. A small departure from the linear trend is also observed at the very beginning of the temperature ramp (from RT to 323 K). This effect might be explained by an experimental uncer-

Table 4 Thermal expansion data for thaumasite

T (K)	a (Å)	c (Å)	V (Å^3)
303	11.0575(1)	10.4163(1)	1102.96(2)
311	11.0581(2)	10.4163(2)	1103.09(3)
317	11.0592(2)	10.4178(2)	1103.45(3)
322	11.0607(2)	10.4192(2)	1103.90(3)
327	11.0618(2)	10.4205(2)	1104.25(3)
332	11.0629(2)	10.4218(2)	1104.62(3)
337	11.0643(2)	10.4233(2)	1105.05(3)
342	11.0654(2)	10.4243(2)	1105.38(3)
347	11.0665(2)	10.4261(2)	1105.78(3)
352	11.0679(2)	10.4277(2)	1106.22(3)
357	11.0691(2)	10.4290(2)	1106.61(3)
362	11.0702(2)	10.4302(2)	1106.98(3)
367	11.0714(2)	10.4317(2)	1107.36(3)
372	11.0726(2)	10.4332(2)	1107.76(3)
377	11.0736(2)	10.4345(2)	1108.11(3)
382	11.0747(2)	10.4360(2)	1108.49(3)
387	11.0760(2)	10.4375(2)	1108.90(3)
392	11.0772(2)	10.4389(2)	1109.28(3)
397	11.0782(2)	10.4403(2)	1109.64(3)
402	11.0796(2)	10.4420(2)	1110.09(3)
407	11.0806(2)	10.4430(2)	1110.40(3)
412	11.0814(2)	10.4438(2)	1110.65(4)
417	11.0825(2)	10.4447(3)	1110.99(4)

tainty (i.e. the assignment of the true temperature to the first heating step) or as due to an initial hysteresis of the cell parameter variation. A remarkable change of the unit cell parameters occurs at about 417 K, thus indicating the amorphization of the mineral.

The mean thermal expansion coefficient over the experimental temperature range from 303 to 417 K was calculated according to Fei (1995). Analyzing our data, we have established that the thermal expansion in the direction parallel to the columns is slightly larger, than in the direction between the columns (Fig. 5). Jacobsen et al. (2003), also reported a similar result, thus indicating that the $[Ca_3Si(OH)_6{\cdot}12\ H_2O]^{4+}$ columns expand in diameter more than they move apart over all the temperature range investigated.

When the temperature is below 333 K, we do not observe any modification in the thaumasite structure; the only remarkable effect is a very small loss of the

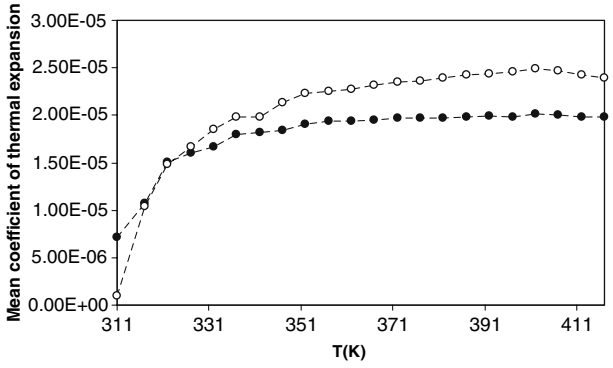

Fig. 5 Mean coefficient of thermal expansion in the temperature range 303–417 K in the direction parallel to the columns (α_c, *white circle*) and between the columns (α_a, *black circle*)

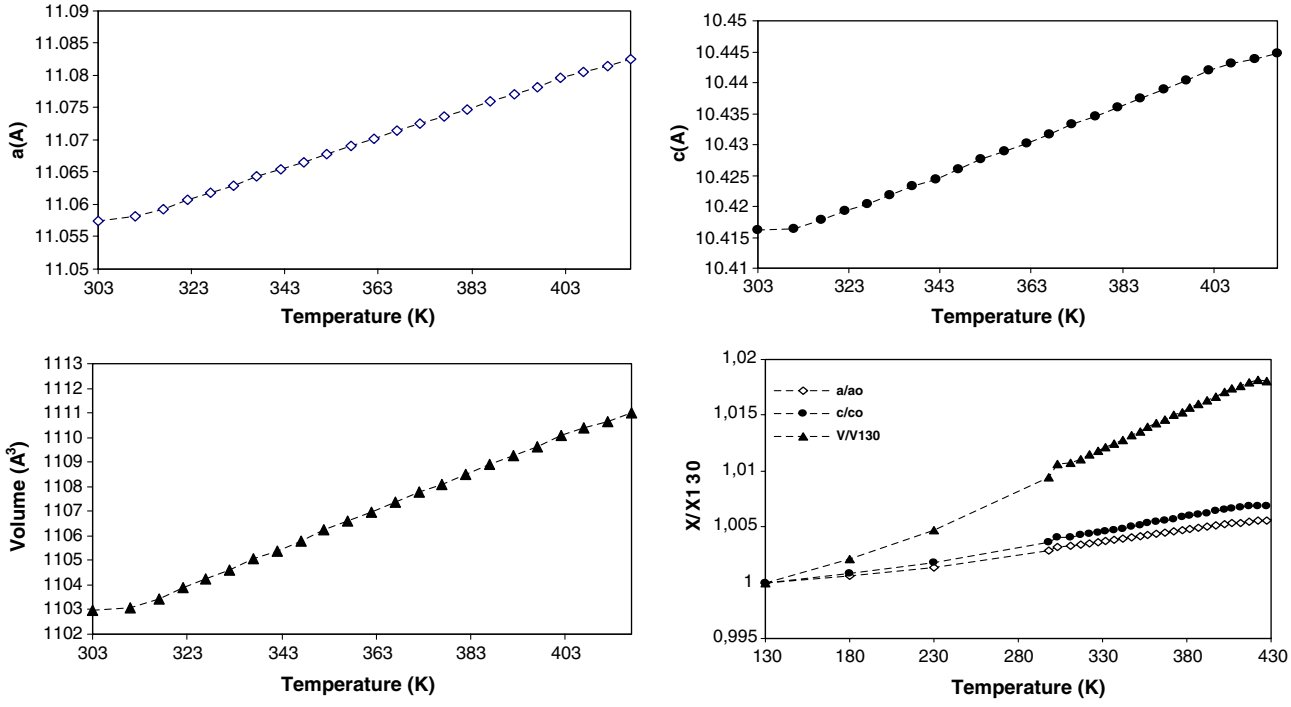

Fig. 4 Temperature dependence of the unit cell parameters of thaumasite. *Error bars* are smaller than symbols

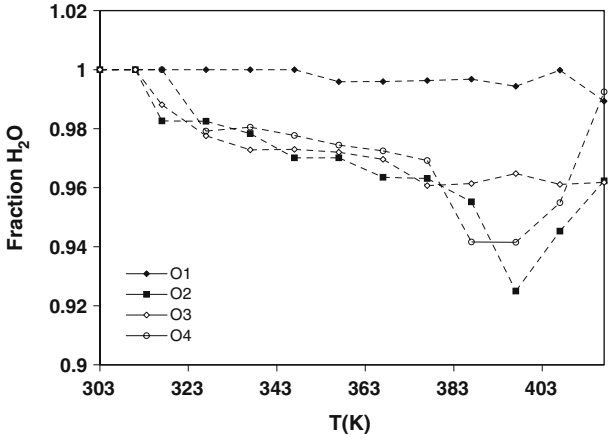

Fig. 6 Variation of occupancy of water molecules, as a function of temperature. *Error bars* are smaller than symbols

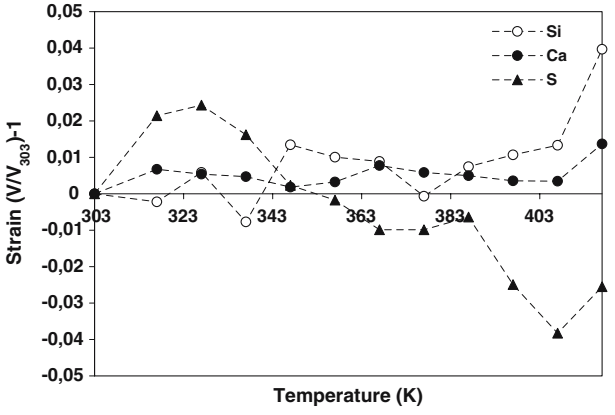

Fig. 7 Thermal expansion of the various components of the thaumasite structure between 303 and 413 K. Volume changes of $[Si(OH)_6]^{2-}$ octahedron (*white circle*), $[Ca_6(H_2O)_4]$ $(OH)_4]^{2-}$ polyhedron (*black circle*) and $(SO)_4^{2-}$ tetrahedron (*black triangle*) are plotted as Lagrangian strain relative to 303 K. *Negative slope* indicates a negative thermal expansion coefficient. *Error bars* are smaller than symbols

water molecules (Fig. 6). The bond lengths do not deviate significantly from their expected range of values, so that the refinements converged to a chemically reasonable crystal structure model without constrains. Variations of the thaumasite structure with temperature are plotted in Fig. 7 in terms of the associated Lagrangian strain relative to the minimum temperature $[(X/X_{303}) -1]$ such that elements with positive thermal expansion have positive slope in Fig. 7. It is very interesting to note that when the $^{VIII}CaO_8$ polyhedron shows positive thermal expansion over all the temperature range investigated, the silicate octahedron shows negative volumetric thermal expansion, and vice versa. This result indicates that the $[Ca_3Si(OH)_6{\cdot}12\ H_2O]^{4+}$ columns are stable over this temperature range and, at the same time, justifies the small increase of the *c* parameter (Fig. 4b).

Our results show that a second dehydration process takes place at about 393 K; above this temperature, the occupancy of water molecules W3 and W4 drops below a level which appears to be critical for the stability of the whole structure (Fig. 6). While losing the crystallization water at this stage, the crystal structure of the mineral collapses and it turns amorphous. This kind of dehydration-induced amorphization of the mineral is confirmed by the TG/DTA analyses reported in Fig. 8. The thermogravimetric curve in flowing nitrogen shows that a much slower weight loss was observed at a temperature lower than 353 K. In the temperature range between 393 and 453 K, a very rapid weight loss took place (~43%) with a maximum rate of 443 K, thus indicating that the dehydration or decomposition of thaumasite is induced by the departure of the crystallization water. This clearly suggests that the stability of thaumasite is mainly governed by the presence of the crystallization water as expected on the basis of its

Fig. 8 TG/DTA analyses in flowing nitrogen for thaumasite

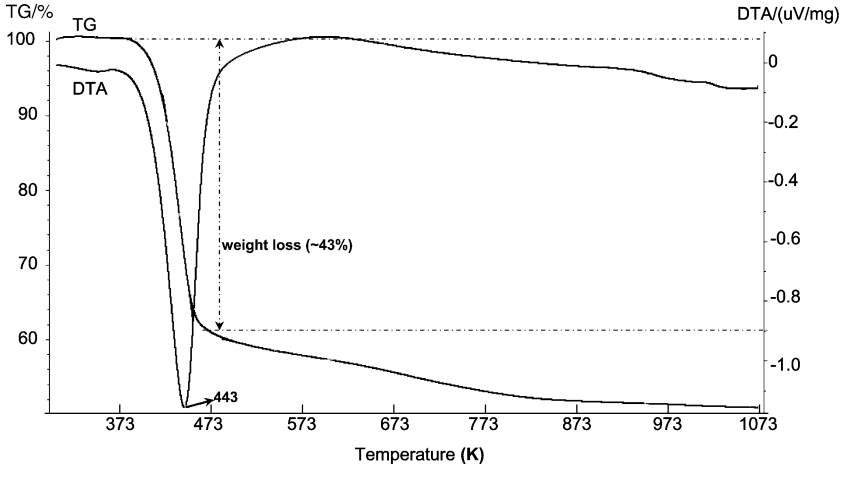

crystal structure. Weight losses at higher temperatures can be attributed to the release of CO_2 and to reactions involving the formation and break-up of sulphate and silico-sulphate phases.

At about 953 K, the appearance of new crystalline material indicates that anhydrite and cristobalite crystallize from the thaumasite glass as shown in Fig. 1.

Conclusions

The high quality of the XRPD data collected during the *in situ* time resolved heating process allowed a careful investigation of the structural changes occurring during decomposition and water removal in thaumasite structure.

Some main points deserve consideration:

1. Thaumasite is stable in the temperature range between 303 and 417 K; the water molecules play a significant role with regard to the thermodynamic properties and occurrence of structural changes in the mineral.
2. Through this temperature range, the cell parameters of thaumasite increase with increasing temperature in a nearly linear fashion up to about 393 K, when a slight slope change is observed.
3. The thermal expansion along the *a*- and *c*-axis directions is very similar in the whole temperature range investigated. The thermal expansion in the direction, parallel to the columns is slightly larger than in the direction between the columns.
4. Our results show that the dehydration process begins at about 333 K and it continues at a slow rate until about 393 K. Above this temperature, the thermogravimetric analysis reveals that the dehydration process proceeds very rapidly while the refined occupancy of water molecules drops below a critical level leading to instability in the thaumasite structure. At the same time, a remarkable change in the unit cell parameters occurring at about 417 K indicates that the crystal structure of thaumasite collapses on losing the crystallization water and it turns amorphous. This result indicates that the dehydration or decomposition of thaumasite is induced by the departure of the crystallization water.
5. At about 953 K, the appearance of new crystalline material indicates that anhydrite and cristobalite crystallize from the thaumasite glass.

Acknowledgments We are indebted to Carlo Meneghini (University of Rome) and Marco Merlini (University of Milan) for their assistance during the experiments at the BM08 (GILDA) beamline (ESRF, Grenoble, France) and the processing of the Translating Imaging Plate data. We thank the referees for the careful reviews and for many useful comments and suggestions. The Italian CNR and INFM are also acknowledged for providing financial support to GILDA and its associated facilities.

References

Angel RJ, Finger LW, Hazen RM, Kanzaki M, Weidner DJ, Liebermann RC, Veblen DR (1989) Structure and twinning of single-crystal $MgSiO_3$ garnet synthesized at 17 Gpa and 1800°C. Am Mineral 74:509–512

Barnett SJ, Adam CD, Jackson ARW (2000) Solid solutions between ettringite, $Ca_6Al_2(SO_4)_3$ $(OH)_{12}{\cdot}26\ H_2O$, and thaumasite $Ca_3SiSO_4CO_3(OH)_6{\cdot}12\ H_2O$. J Mater Sci 35:4109–4114

Bensted J (1999) Thaumasite—background and nature in deterioration of cements, mortars and concretes. Cem Concr Compos 21:117–121

Brough AR, Atkinson A (2001) Micro-Raman spectroscopy of Thaumasite. Cem Concr Compos 31:421–424

Carpenter AB (1963) Oriented overgrowths of Thaumasite on Ettringite. Am Miner 48:1394–1396

Crammond NJ (1985) Thaumasite in failed cement mortars and renders from exposed brickwork. Cem Concr Res 15:1039–1050

Drábik M, Gáliková L (2003) Method of thermal analysis in the detection of thaumasite and its presence in the sulphate-attacked concrete. Solid State Phenomena 90–91:33–38

Edge RA, Taylor FW (1971) Crystal structure of Thaumasite, $[Ca_3Si(OH)_6{\cdot}12\ H_2O](SO_4)(CO_3)$. Acta Cryst B27:594–601

Effenberger H, Kirfel A, Will G, Zobetz E (1983) A further refinement of the crystal structure of thaumasite, $Ca_3Si(OH)_6CO_3\ SO_4{\cdot}12\ H_2O$. N Jb Miner Mh 2:60–68

Federico M (1970) Un inconsueto deposito di thaumasite fra i tufi del cratere di Prata Porci (Colli Albani). Miner Mag 32:567–572

Fei Y (1995) AGU reference shelf 2: mineral physics and crystallography—a handbook of physical constants. In: Ahrens TJ (ed) AGU, Washington, pp 29–44

Font-Altaba M (1960) A thermal study of thaumasite. Mineral Mag 32:567–572

Frost DJ, Fei Y (1998) Stability of phase D at high pressure and high temperature. J Geophys Res 103:7463–7474

Giampaolo C (1986) Dehydration kinetics of thaumasite at ambient pressure. N Jb Miner Mh Jg H 3:126–134

Granger MM, Protas J (1969) Détermination et étude de la structure crystalline de la jouravskite $Ca_3Mn^{IV}(SO_4)(CO_3)(OH)_6{\cdot}12\ H_2O$. Acta Crystallogr B 25:1943–1951

Grubessi O, Mottana A, Paris E (1986) Thaumasite from the Tschwinning [N'Chwaning] mine, South Africa. Tschermaks Mineral Petrog Mitt 35:149–156

Horiuchi H, Hirano M, Ito E, Matsui Y (1982) $MgSiO_3$ (ilmenitetype): single-crystal X-ray diffraction study. Am Mineral 67:788–793

Horiuchi H, Ito E, Weidner DJ (1987) Perovskite-type $MgSiO_3$: single-crystal X-ray diffraction study. Am Mineral 72:357–360

Hurlbut CS, Baum JL (1960) Ettringite from Franklin, New Jersey. Am Mineral 45:1137–1143

Jacobsen SD, Smyth JR, Swope RJ (2003) Thermal expansion of hydrated six-coordinate silicon in thaumasite, $Ca_3Si(OH)_6(CO_3)(SO_4)\ 12\ H_2O$. Phys Chem Miner 30:321–329

Kirov GN, Poulieff CN (1968) On the infra-red spectrum and thermal decomposition products of thaumasite, $Ca_3H_2(CO_3/SO_4)SiO_4{\cdot}13\ H_2O$. Mineral Mag 36:1003–1011

Knill DC (1960) Thaumasite from County Down, Northern Ireland. Mineral Mag 32:416–418

Lachaud R (1979) Thaumasite and ettringite in construction materials. Annales de l'Institut du Batiment et des Travaux Publics 32:370–373

Larson AC, Von Dreel RB (2000) GSAS general structure analysis system. Report LAUR. Los Alamos National Laboratory, Los Alamos, pp 86–748

McDonald AM, Peterson OV, Gault RA, Johnsen O, Niedermayr G, Branstätter F (2001) Micheelsenite, $(Ca, Y)_3Al(PO_3OH, CO_3)(CO_3)(OH)_6{\cdot}12\,H_2O$, a new mineral from Mont Saint-Hilaire, Quebec, Canada and the Nanna pegmatite, Narsaarsuup Qaava, South Greenland. Neues Jahrbuch Mineralogie Monatshefte 8:337–351

Merlino S, Orlandi P (2001) Carraraite and zaccagnaite, two new minerals from the Carrara marble quarries: their chemical compositions, physical properties, and structural features. Am Mineral 86:1293–1301

Noack Y (1983) Occurrence of thaumasite in a seawater–basalt interaction, Mururoa atoll (French Polynesia, South Pacific). Mineral Mag 47:47–50

Norby P (1997) Synchrotron powder diffraction using imaging plates: crystal structure determination and Rietveld refinement. J Appl Cryst 30:21–30

Peters JJ (1984) Triassic Traprock minerals of New Jersey. Rocks Miner 59:157–183

Reeder RJ (1983) Crystal chemistry of the rhombohedral carbonates. In: Reeder RJ (ed) Carbonates: mineralogy and chemistry. Reviews in mineralogy, vol 11. Mineralogical Society of America, pp 1–47

Ross NL, Shu JF, Hazen RM (1990) High-pressure crystal chemistry of stishovite. Am Mineral 75:739–747

Vogt T (1938) Thaumasite from Sulitelma, Norway. Norsk Geol Tidskr 18:291–303

Yang H, Prewitt CT, Frost DJ (1997) Crystal structure of the dense hydrous magnesium silicate, phase D. Am Mineral 82:651–654

Zemann J, Zobetz E (1981) Do the carbonate groups in thaumasite have anomalously large deviations from coplanarity? Kristallografija 26:1215–1217